

Customized Synthesis: Solvent- and Acid-Assisted Topology Evolution in Zirconium-Tetracarboxylate Frameworks

Hai-Lun Xia, Kang Zhou, Liang Yu, Hao Wang, Xiao-Yuan Liu,* Davide M. Proserpio, and Jing Li*



Cite This: *Inorg. Chem.* 2022, 61, 7980–7988



Read Online

ACCESS |



Metrics & More

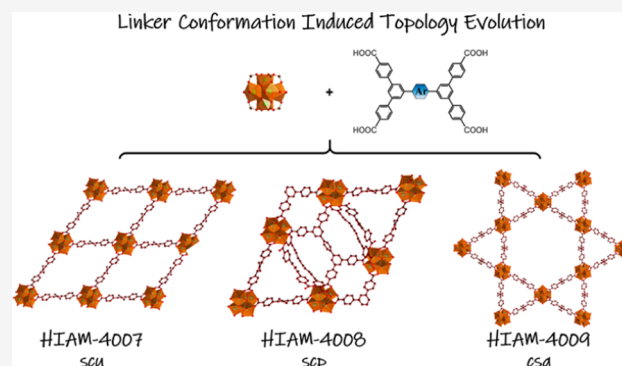


Article Recommendations



Supporting Information

ABSTRACT: Metal–organic frameworks (MOFs) demonstrate strong potential for various important applications due to their well tunable structures and compositions through metal and organic linker engineering. As an effective approach, topology evolution by controlling linker conformation has received considerable attention, where solvents and acids have crucial effects on structural formation. However, a systematic study of such effects remains under investigated. Herein, we carried out a methodical study on the topology evolution in Zr-MOFs directed by solvothermal conditions with various combinations of three common solvents and six different acids. As a result, three Zr-MOFs with different topologies, **scu** (HIAM-4007), **scp** (HIAM-4008), and **csq** (HIAM-4009), were obtained using the same Zr_6 -cluster and tetratopic carboxylate linker, in which structure diversity shows significant influence on their corresponding photoluminescence quantum yields. Further experiments revealed that the acidity of acids and the basicity of solvents strongly influenced the linker conformation in the resultant MOFs, leading to the topology evolution. Such a solvent- and acid-assisted topology evolution represents a general approach that can be used with other tetratopic carboxylate linkers to realize structural diversity. The present work demonstrates an effective structure designing strategy by controlling synthetic conditions, which may prove to be powerful for customized synthesis of MOFs with specific structure and functionality.



INTRODUCTION

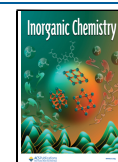
Metal–organic frameworks (MOFs) are a category of hybrid porous materials built of inorganic metal ions/clusters and organic linkers through coordination bonds.^{1,2} Tunable structures of MOFs give rise to diversity of structures and functionalities, which allow them to be customized for a wide variety of important applications, including but not limited to gas storage and separation,^{3,4} luminescence-based sensing and photonics,^{5,6} and heterogeneous catalysis.^{7,8} So far, some 100 000 MOF compounds have been reported,⁹ offering a large pool of functional materials for target-specific applications and devices.¹⁰ To make them ready for commercialization, directional synthesis of customized MOF structures signifies the next stage of the MOF development.¹¹

Assembly of various metal ions/clusters and organic linkers confers the diversity of MOFs. Three strategies have been commonly utilized for customized MOF synthesis. As shown in Scheme 1, (i) linker engineering is a powerful way to introduce specific properties or new functions to MOFs.^{12–16} For example, UiO-66, UiO-67, and UiO-68 possess the same topology with increased pore size as a result of increasing ligand length.¹⁷ The same strategy has been used to prepare a MOF-74 series with large-pore apertures.¹⁴ Additionally, pre- and post-synthesis linker modification^{16,18,19} and linker installation^{20–24} have also been proven to be useful approaches

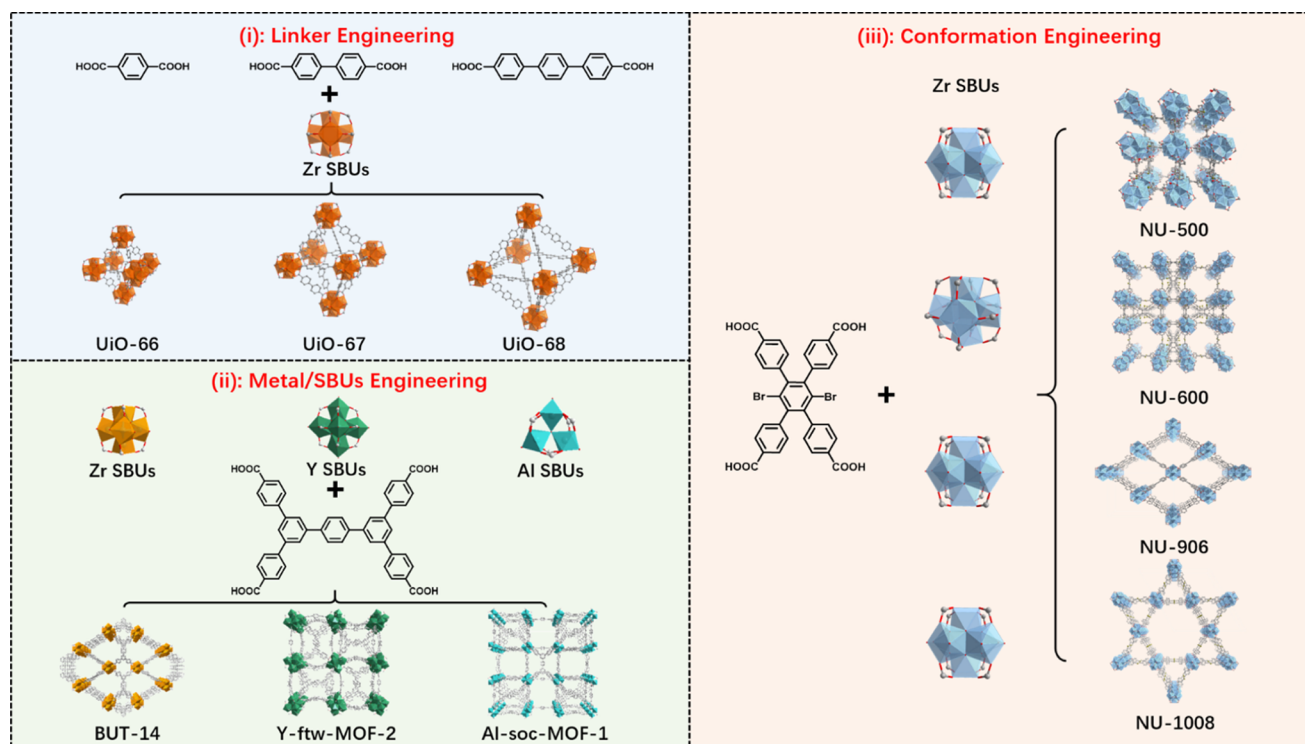
to achieve target-specific properties on resultant MOFs. (ii) Metal/ secondary building unit (SBU) engineering is another strategy to create the structure diversity in MOFs.²⁵ Assembly of different SBUs with the same linker results in different underlying nets.^{26,27} For instance, the simplest and rigid ditopic terephthalic acid, H_2bdc , is the first organic linker adopted in MOF synthesis. It has been used to connect with several metal nodes, such as Zr, Zn, Al, Cr, and Ti SBUs, to form UiO-66,¹⁷ MOF-5,^{28,29} MIL-53,³⁰ MIL-101,³¹ and MIL-125,³² respectively, to name a few. Varying structures, like BUT-14,⁴² Y-ftw-MOF-2,³³ and Al-soc-MOF-1,³⁴ could be formed when Zr, Y, and Al were used as the metal source, respectively, and 3,3'',5,5''-tetrakis(4-carboxyphenyl)-*p*-terphenyl was used as the organic linker (Scheme 1). Strategies mentioned above concentrate on the diversity of linkers and SBUs, which leads to a very rich MOF structural database. On the other hand, other structure-directing parameters also exist,

Received: February 26, 2022

Published: May 9, 2022



Scheme 1. Schematic Representation of the Three Strategies for Customized MOF Synthesis: (i) Linker Engineering, (ii) Metal/SBUs Engineering, and (iii) Conformation Engineering



such as molecular stretching and twisting of the linkers, that often give rise to different conformations. They also play an important role in the topology of the final structures of MOFs. These parameters can be controlled by varying synthetic conditions, including the solvent and acid modulator.^{35,36} This strategy is categorized as (iii) linker conformation engineering (Scheme 1). A suitable combination of the solvent and modulating chemical species can directly affect the conformation of linkers, resulting in different nets with the same linker and metal node.³⁷

Tetrapotic carboxylates are good candidates of linkers to generate conformation-dependent topologies compared with tricarboxylic and dicarboxylic acid-based linkers. For example, as one of the most extensively studied linkers, tetrakis-(4-carboxyphenyl)porphyrin (H₄TCPP) has been reported to form several topologies with Zr₆ clusters,³⁸ where the underlying net is determined by the conformation of TCPP and the connectivity of the Zr₆ cluster controlled by various synthetic conditions. In addition, as a useful strategy to influence the linker conformation, steric hindrance has been introduced into the linker backbone to control the nets of resulting MOFs.³⁹ Zhou and co-workers systematically studied a series of (4,8)-c Zr-tetracarboxylate-based MOFs by changing the substituents on different positions of the tetrapotic carboxylate linkers.⁴⁰ Tunable linker rotamers lead to three types of structures with **csq**, **flu**, and **scu** topologies underlying nets under controllable solvothermal conditions. These results indicate that rationally selecting the modulators and solvent serves as an effective way in directing MOF structures. However, to this date, there is lack of studies to systemically study the relationship between them.

In a recent report, Farha and co-workers studied the solvent and acid effect on the topologies of resultant Zr-MOFs using 1,4-dibromo-2,3,5,6-tetrakis (4-carboxyphenyl) benzene

(H₄TCPB-Br₂) as the linker.³⁷ Two kinds of solvents (*N,N*-dimethyl formamide, DMF; *N,N*-diethyl formamide, DEF) and two types of acid modulators (formic acid, FA; acetic acid, AA) were investigated. By precisely modulating the synthetic conditions, the connectivities of the Zr₆ cluster and the conformations of the TCPB-Br₂ can be simultaneously controlled. As a result, four different topologies were obtained, that is, a new 4,4,4,5-coordinated tetranodal net (NU-500), 4,6-c **she** (NU-600), 4,8-c **scu** (NU-906), and 4,8-c **csq** (NU-1008), as shown in Scheme 1.

Very recently, we have also prepared a series of Zr-MOFs HIAM-400X (HIAM = Hoffmann Institute of Advanced Materials, 40 = Zirconium, X = 0–4) using a similar tetracarboxylic acid linker.²¹ One **scu** net, same as NU-906, was obtained in the DMF solvent with benzoic acid (BA) as the acid. An interesting question is would it be possible to attain other nets when different solvents and acids are utilized. To explore such possibilities and to understand how reaction conditions affect important structural parameters that govern topological evolution, such as linker conformation and SBU connectivity, we carried out a systematic study to synthesize a series of Zr-MOFs composed of the same tetracarboxylate linker under various combinations of solvents and acids and to evaluate the mechanism of topological evolution of MOFs formed under different reaction conditions.

RESULTS AND DISCUSSION

Solvent- and Acid-Assisted Topology Evolution of Zr-Tetracarboxylate Frameworks. Based on the aforementioned considerations, we first designed and synthesized a linker, 5',5'''-(2,3-diaminophenyl)-bis{[(1,1':3',1''-terphenyl)-4,4''-dicarboxylic acid]} (APTC), similar to that used in HIAM-400X (X = 0–4) via Suzuki reactions and followed hydrolysis under mild conditions as shown the Supporting

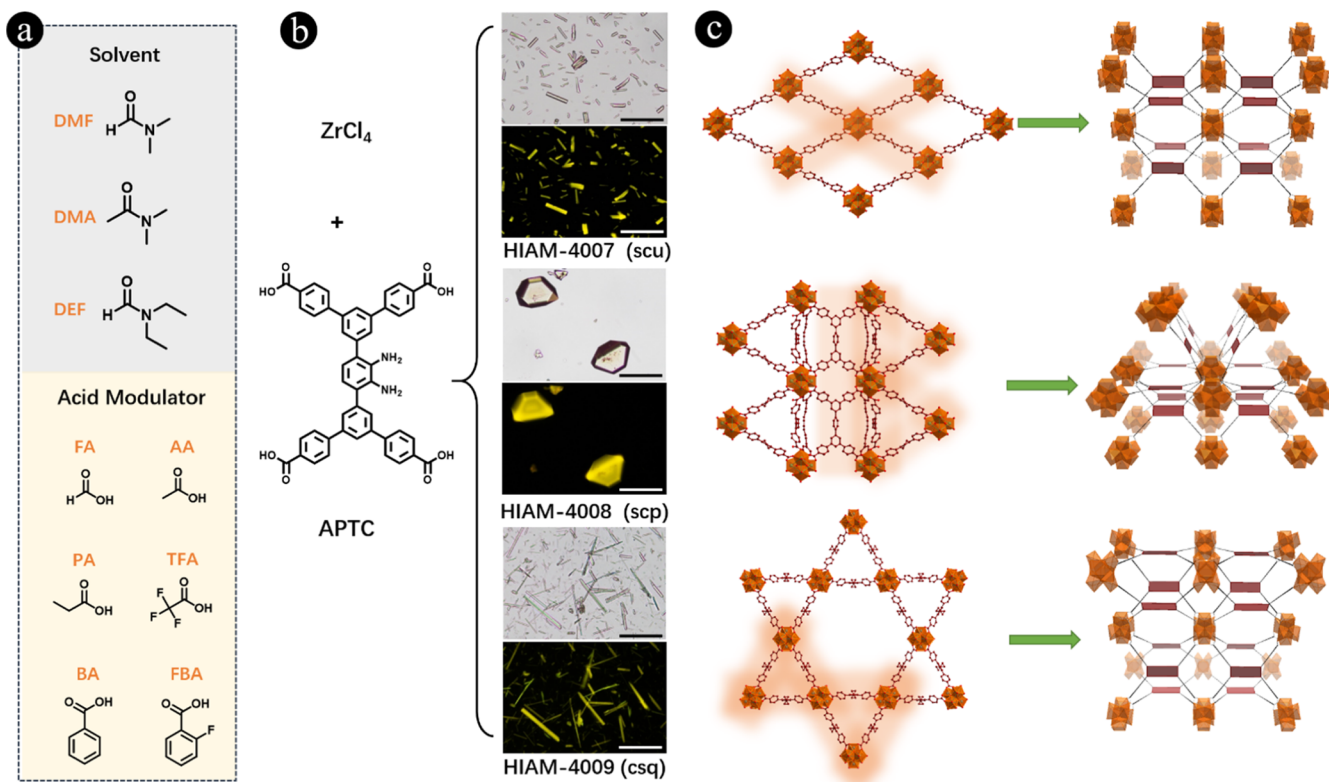


Figure 1. (a) Molecular structure of three solvents and six different acid modulators employed for MOF synthesis; (b) schematic representation of the preparation and the single crystal images of HIAM-4007, HIAM-4008, and HIAM-4009 under daylight and 450 nm excitation (scale bar: 100 μm); and (c) single crystal structure of HIAM-4007, HIAM-4008, and HIAM-4009 (Color scheme: C, brown; O, red; and Zr, green. H and N atoms in the structures are omitted for clarity).

Information. Similar linkers have been utilized to prepare Zr-MOFs with **scq** and **csq** topology under different solvothermal conditions.^{21,41,42} To systematically study the effects of the solvent and acid on the topology evolution of Zr-MOFs, three solvents, DEF, *N,N*-dimethyl acetamide (DMA), and DMF, were selected along with six different acids, namely BA, 2-fluorobenzoic acid (FBA), FA, AA, propionic acid (PA), and trifluoroacetic acid (TFA) as modulators (see Figure 1a). To avoid temperature- and reaction time-induced structure diversity, the synthetic temperature was fixed at 120 $^{\circ}\text{C}$, and the reaction time was fixed for 3 days. By various combinations of the selected solvents and acids, the reactions of ZrCl_4 (metal source) and APTC (linker) resulted in three structures: HIAM-4007 (**scu**), HIAM-4008 (with the new trinodal 4,4,12-**c scp** net), and HIAM-4009 (**csq**)²⁰ as shown in Figure 1b,c. The detailed synthesis conditions are listed in Table S1. These results indicate that the structures and topologies of the Zr-based MOFs can indeed be tuned through suitable choice of the solvent and modulator.

Structural Analysis and Description of HIAM-4007, HIAM-4008, and HIAM-4009. Prismatic crystals of HIAM-4007 were obtained by the solvothermal reaction of ZrCl_4 and APTC in DMF with BA serving as the modulator, which was similar to the synthetic procedure for HIAM-4000. Single crystal X-ray diffraction (SC-XRD) analysis revealed that HIAM-4007 crystallized in the orthorhombic crystal system with the *Cmmm* space group (Table S2). Each Zr_6O_8 cluster is coordinated by eight fully deprotonated APTC linkers and eight terminal $\text{H}_2\text{O}/\text{OH}^-$ groups. Each APTC is connected to four Zr_6 clusters, leading to a (4,8)-**c scu** net in HIAM-4007 (Figure 1c). These data give the overall formula of HIAM-

4007 as $\text{Zr}_6\text{O}_4(\text{OH})_8(\text{H}_2\text{O})_4(\text{APTC})_2$. Four types of one-dimensional (1D) open channels are formed, that is, rhombic channels and hexagonal channels along the *a*-axis and two different rhombic channels along the *b*- and *c*-axis (Figure S1). The permanent porosity of HIAM-4007 was examined by N_2 sorption isotherms at 77 K with a Brunauer–Emmett–Teller (BET) surface areas of 496.1 m^2/g and a total pore volume of 0.206 cm^3/g (Figure S2).

The solvothermal reaction of the ZrCl_4 and APTC linker using DEF as the solvent and AA as the modulator yielded truncated octahedral crystals of HIAM-4008. The SC-XRD analysis indicated that HIAM-4008 crystallizes in the tetragonal crystal system with the *I4₁/amd* space group (Table S3). HIAM-4008 also possesses the Zr_6O_8 cluster, but each Zr_6 cluster is coordinated by 12 APTC linkers and 4 terminal $\text{H}_2\text{O}/\text{OH}^-$ groups, leading to a new trinodal (4,4,12)-**c scp** net in HIAM-4008 (Figures 1c and S3). In this structure, eight APTCs are coordinated with the Zr_6 cluster via a bidentate carboxylate group, while the other four APTCs are disorder over two positions (50–50%). The disordered APTC is monodentate to the Zr_6 cluster (Figure S4). From a topological viewpoint, the connectivity of the Zr_6 node increases from 8 in HIAM-4007 to 12 in HIAM-4008 by changing the solvent and acid, while all APTC linkers connect always four Zr_6O_8 clusters. The formula of HIAM-4008 thus is $\text{Zr}_6\text{O}_4(\text{OH})_4(\text{H}_2\text{O})_4(\text{APTC})_3$. Three types of 1D open channels are formed, namely, triangle channels, trapezoid channels, and rhombic channels along both the *a*-axis and *b*-axis, while no open channels are formed along the *c*-axis (Figure S3). The BET surface areas and total pore volume are

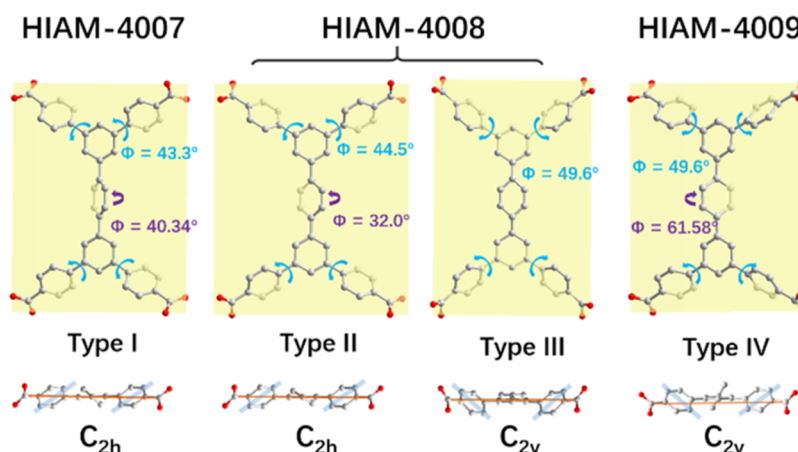


Figure 2. Twisting of the phenyl rings in the different conformations of the APTC linker in HIAM-4007, HIAM-4008, and HIAM-4009.

1903.9 m²/g and 0.687 cm³/g for HIAM-4008, respectively (Figure S5).

Thinner and longer prismatic crystals of HIAM-4009 were obtained via the solvothermal reaction of the ZrCl₄ and APTC linker in DEF with BA as the modulator. The prismatic single crystals of HIAM-4009 (csq) are not large enough for SC-XRD analysis. Topology of HIAM-4009 was determined by comparing the structures of HIAM-4009 and the similar Zr-MOF, PCN-808, with the overall formula of Zr₆O₄(OH)₈(H₂O)₄(APTC)₂.²¹ Each Zr₆ cluster in HIAM-4009 is coordinated by eight fully deprotonated APTC linkers and eight terminal H₂O/OH[−] groups (Figure 1c). Each APTC is connected to four Zr₆ clusters to form a (4,8)-c csq topology in HIAM-4009, different from scu found for HIAM-4007. Two types of one-dimensional open channels are formed along the *c*-axis, that is, one triangle channel and one hexagonal channel (Figure S6). The corresponding BET surface areas and total pore volume are 1294.9 m²/g and 0.759 cm³/g for HIAM-4009, respectively (Figure S7). According to the N₂ sorption data, the pore size distribution-based density functional theory method indicated hierarchically porous structures with micropores at 14.1 Å and mesopores at 26.6 Å for HIAM-4009 (Figure S7).

For tetratopic carboxylic acid-based MOFs, other topologies were also reported, such as (4, 12)-c ftw, (4,8)-c sqc, and (4,8)-c flu. However, we did not obtain these structures in our study, which might be contributed to the following facts: (i) the Zr₆-based ftw net has strict demands on the linker size, i.e., the aspect ratio;⁴³ (ii) the (4,8)-c sqc net might be prepared after removing the two independent APTCs from the (4, 4, 12)-c scp net, as reported by Prof. Yang's group;⁴² and (iii) the flu net needs the linkers with tetrahedral conformation.⁴⁰

Linker Conformation Analysis in Different MOFs. As mentioned earlier, molecular stretching and twisting commonly exist in MOF structures, and often, they determine the final topology of MOFs. In our work, no steric hindrance was introduced into the linker backbone, and the amount of the ZrCl₄/APTC linker (23.3 mg/10 mg) and reaction temperature/time (120 °C/3 days) were all kept constant, while the type and amount of the solvent and modulator were varied. In addition, all three structures (HIAM-4007, HIAM-4008, and HIAM-4009) are composed of the same Zr₆ clusters (SBUs). Therefore, the conformations of the APTC linker played a dominating role in the final topology in these structures.

The conformations of the APTC linkers in the three Zr-MOFs are depicted in Figure 2. For the purpose of clarity, both amino groups on the phenyl ring are omitted. The linkers in the (4,8)-c scu net of HIAM-4007 display only one crystallographic conformation (type I), with a C_{2h} symmetry. Both pairs of the adjacent phenyl arms rotate 43.3° in the same direction. In the (4,8)-c csq net of HIAM-4009, the APTC linkers also display only one crystallographic conformation. Different from that in HIAM-4007, the linker here has a C_{2v} symmetry (type IV), in which two adjacent phenyl arms rotate away from each with the same angle of 49.6°. Interestingly, the linkers in HIAM-4008 display both crystallographic conformations (type II and type III) similar to type I and type IV. It is worth noting that only the APTC linkers displayed on the plane between the *a*-axis and *b*-axis have the conformation with the C_{2v} symmetry, in which two adjacent phenyl arms rotate away from each with the same angle of 49.6°. The other type of APTC linker possesses the C_{2h} symmetry, in which both pairs of the adjacent phenyl arms rotate 44.5° in the same direction. Thus, the twisting of phenyl rings within APTC linker conformations determines the topologies in resulting HIAM-4007, HIAM-4008, and HIAM-4009.

Structure Effect on Photoluminescent Properties. As shown in Figure S8, similar photoluminescence, UV–vis absorption, and thermogravimetric analysis behaviors were observed for HIAM-4007, HIAM-4008, and HIAM-4009. However, due to varying linker conformations and packing in different nets, the interactions between linkers will be influenced. As a result, different photoluminescence quantum yields (PLQYs) were recorded for these three MOFs. The PLQYs are 6.1, 2.8, and 5.7% under 450 nm excitation for HIAM-4007, HIAM-4008, and HIAM-4009, respectively. The lowest PLQY for HIAM-4008 could be ascribed to the fact that the (4,4,12)-c scp net has the highest linker density compared with (4,8)-c scu and csq nets, which will lead to the severest aggregation-cause luminescence quenching. In addition, as seen from the single crystal analysis, organic linkers in (4,8)-c csq HIAM-4009 (Figures 1C, S1, and S4) possess stronger π – π stacking interactions than those in (4,8)-c scu HIAM-4007, which will result in a higher PLQY for HIAM-4007 than that of HIAM-4009. These results demonstrate that MOF structures have a significant effect on their photoluminescent properties, in which acid- and solvent-assisted topology evolution could be used as a useful method for customized synthesis of MOFs with the highest performance.

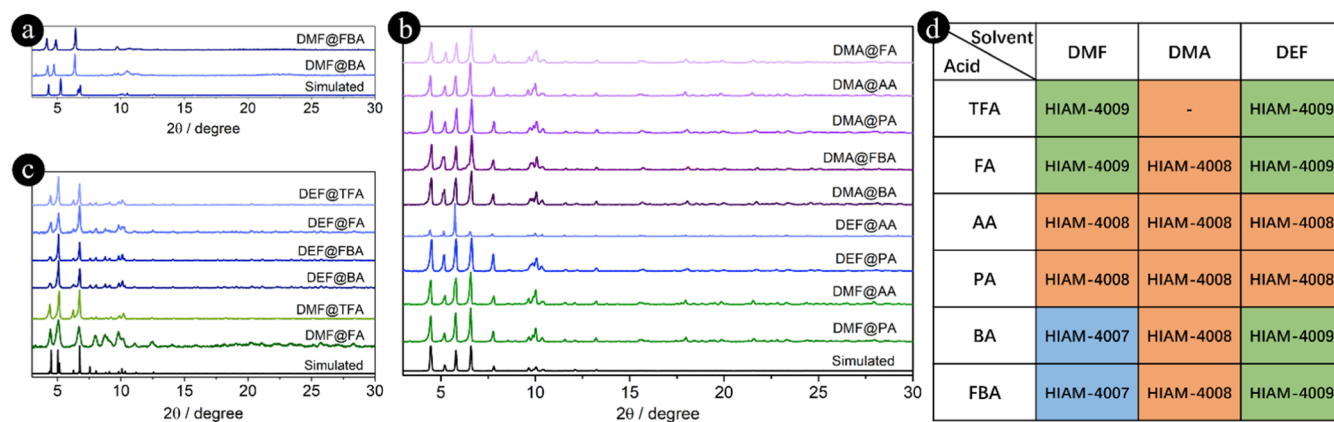


Figure 3. PXRD patterns of HIAM-4007 (a), HIAM-4008 (b), and HIAM-4009 (c) synthesized under different solvothermal conditions (d).

Characterization of MOFs Synthesized Using Different Solvents and Acids. As aforementioned, the linker conformation and consequently the topology of MOFs vary with different combinations of solvents and acids. Table S1 summarizes the details of such combinations using three types of solvents (DEF, DMA, and DMF) and six acid modulators (BA, FBA, FA, AA, PA, and TFA). The results show that adjusting the ratio of the acid modulator had a slight effect on the topology, while several exceptions were observed when a much lower or higher concentration of acids was used (Table S1, Figures S9–S14). Therefore, only crystals obtained with a mid-concentration of each acid modulator were further analyzed. Images of all crystal samples are summarized in Figures S9–S11. The phase purities of HIAM-4007, HIAM-4008, and HIAM-4009 were confirmed by the excellent agreement between the experimental powder X-ray diffraction (PXRD) patterns and the simulated ones generated from the corresponding single crystal diffraction data.

In the case of HIAM-4007, as observed in Figure 3a,d, there are only two kinds of combinations that resulted in this topology. In both cases, DMF was used as the solvent with BA or FBA as acid modulators. There are notable peak shifts in the PXRD patterns for both dried crystals, due to their structural flexibility. In the case of HIAM-4008, nine different combinations generated this topology (Figure 3b,d). Finally, six combinations succeeded in producing HIAM-4009. It was notable that highly crystalline samples were obtained either in DEF or with TFA/FA as acid modulators (Figure 3c,d). The PXRD analysis also suggests that combinations of DMF and FA generally resulted in less-crystalline samples. Based on the data shown in Figure 3d, it is also clear that reactions with DMA as the solvent yielded exclusively HIAM-4008, regardless of what acid was used, except TFA, which as a modulator, yielded almost no crystals, and adjusting its amount also had no effect. In the case of DMF, all three types of Zr-MOFs can be synthesized. HIAM-4007 was obtained when BA and FBA were used; HIAM-4008 was prepared using AA and PA as the modulators, while HIAM-4009 was obtained when TFA and FA were utilized. However, in the case of DEF, only two types of Zr-MOFs could be achieved. Considering acid modulators, use of AA and PA only resulted in HIAM-4008. Variation of solvents had no effect on the MOF topology. HIAM-4007 only occurred when BA or FBA was employed as acid modulators and DMF as the solvent.

All above-mentioned results demonstrate that the selection of the solvent and acid modulator directly affect the resulting

linker conformation and MOF structure. The topology of the Zr-MOFs built on the same linker and identical Zr_6 cluster can be controlled by solvents and acid modulators.

Mechanism of Topology Evolution of Different MOFs.

To understand the factors that contribute to various conformations of APTC in HIAM-4007,8,9, we investigated the further possible mechanism of crystal formation. The results from the previous section demonstrate that the topology evolution from HIAM-4007 to HIAM-4009 was controlled solely by the choices of solvents and acids used in the synthesis, which directed to different linker conformations in the final crystal structures. It is well known that the pK_a of an acid has a significant effect on the nucleation and crystal growth by competing with linkers for coordination sites on Zr_6 clusters to terminate the coordination process and to form Zr_6 nodes with lower connectivity.^{37,38,44,45} Solvents with different physical and chemical properties also influence the nucleation and crystal growth processes by altering the solubility of the organic linkers and the degree of interaction with acids.⁴⁶ Therefore, we carried out a systematic comparison of the acidity of the modulating acids and the basicity of solvents to understand their effect on the topology evolution.

The pK_a values of all the solvents and modulators used in this study are summarized in Table 1.^{47–50} As seen from the

Table 1. pK_a of Acids and Solvents Used in This Study

Acid	pK_a	solvent	pK_a
TFA	0.3	DMF	−0.70
FBA	3.6		
FA	3.7	DEF	−0.50
BA	4.2		
AA	4.8	DMA	0.10
PA	4.9		

table, the pK_a of modulators increases in the order of TFA, FBA, FA, BA, AA, and PA. As has been observed, AA and PA lead to the HIAM-4008 structure, which is a (4,4,12)-c scp underlying net. As reported previously, the modulator with higher pK_a would lead to a weaker competition with the linker for coordinating with the Zr_6 cluster, thereby giving rise to higher connectivity of the metal nodes in the resulting MOFs.³⁷ Accordingly, in the case of AA and PA with the highest pK_a values among the selected acid modulators, HIAM-4008 with fully connected nodes was obtained, regardless of which solvent was used. On the contrary, for

the acid modulators with lower pK_a values such as BA, FA, FBA, and TFA, (4,8)-c **scu** and **csp** nets with lower connectivity resulted in HIAM-4007 and HIAM-4009 with DEF or DMF employed as the solvent.

Interestingly, FBA has a similar pK_a to FA, indicating that the competitiveness of FA and FBA toward the APTC linker for coordinating with the Zr_6 node should be similar. However, different structures resulted in DMF. HIAM-4009 was obtained with FA, while HIAM-4007 was acquired with FBA. In HIAM-4007, a rhombic-shaped channel along the c -axis is observed, while two types of one-dimensional open channels are formed in HIAM-4009 along the c -axis: a triangle-shaped channel and hexagon-shaped channel (Figures S1 and S6). Notably, this additional smaller triangle-shaped channel is formed in HIAM-4009. Considering the steric hindrance of the two acids, FBA possesses a larger molecular size than FA. Thus, it might be difficult for FBA to form a small triangular channel to form HIAM-4009. Accordingly, a monotonous rhombic-shaped channel was formed in HIAM-4007, while the smaller sized FA gives rise to the coordination diversity in HIAM-4009, giving rise to two types of one-dimensional open channels.

Considering the solvent effect, only one type of MOF, namely HIAM-4008, was obtained in DMA, while all three types of MOFs could be synthesized in DMF, and two types of MOFs, HIAM-4008 and HIAM-4009, can be crystallized in DEF. Since the APTC linker dissolves completely in all three solvents, polarity of the solvents plays little role and, thus, is not studied here. The basicity of the three solvents was considered. The basicity increases in the order of DMF, DEF, and DMA. DMA shows the strongest basicity, which will weaken the competition of the acid with the linker for coordinating with the Zr_6 cluster, leading to the higher connectivity of the Zr_6 cluster. The basicity of DEF was stronger than that of DMF but weaker than that of DMA, resulting in two topologies. With the weakest acids, AA and PA, HIAM-4008 with higher connectivity was formed using DEF as the solvent. With the increased acidity, the HIAM-4009 with lower connectivity was obtained. The synthetic process became extremely complicated when DMF was used as the solvent, which involved deprotonation of linkers, interaction between the solvent and acid, and the competition between the acid and linker for coordinating with the Zr_6 cluster. DMF has the lowest basicity; thereby, the acid with different acidity will have a significant effect on the crystal nucleation and growth. As a result, three topologies were generated. All above-mentioned results demonstrate that the solvents and acids controlled the topologies of MOFs synergistically. Either the solvent or acid plays an important role in determining the topologies of Zr-MOFs when their pK_a values are extremely low or high.

Topology Control Using Different Tetratopic Carboxylate Linkers. As mentioned earlier, only one type of topology was obtained for HIAM-4001 and HIAM-4003 in our previous study.²² In order to verify the proposed mechanism, we used the similar linkers $5',5'''$ -(benzo[*c*]-[1,2,5]thiadiazole-4,7-diyl)bis((1,1':3',1''-terphenyl)-4,4''-dicarboxylic acid)) (BTTC) and $5',5'''$ -(naphtho[2,3-*c*][1,2,5]thiadiazole-4,9-diyl)bis((1,1':3',1''-terphenyl)-4,4''-dicarboxylic acid)) (NTTC), see Figure 4a but different solvents and acids to test out whether new types of Zr-MOFs can be obtained. AA and BA were adopted as the acid modulators,

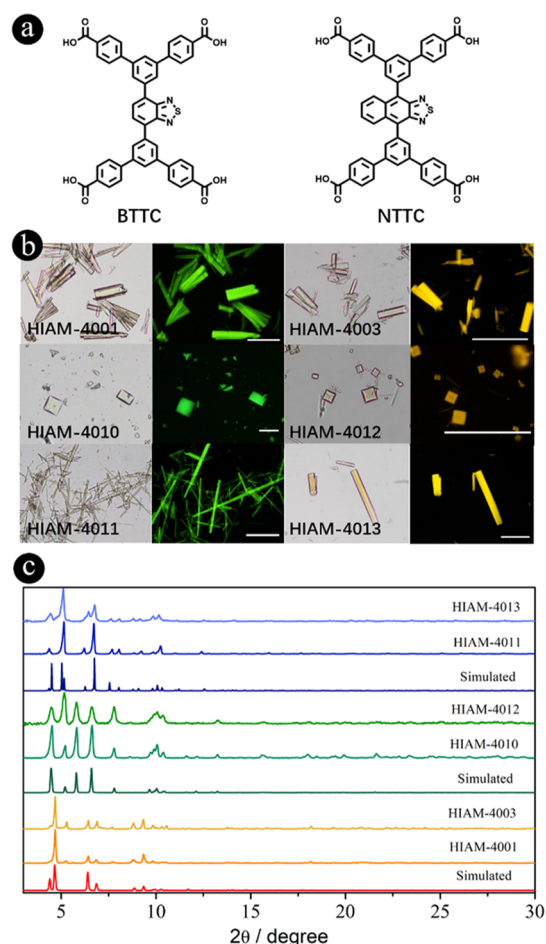


Figure 4. (a) Structures of the tetracarboxylic acid ligand BTTC and NTTC used in the synthesis of HIAM-4001 and HIAM-4003. (b) Single crystal images of HIAM-4001, HIAM-4010, HIAM-4011, HIAM-4003, HIAM-4012, and HIAM-4013 under daylight (left) and 450 nm photoexcitation (right, scale bar: 100 μ m). (c) PXRD patterns of HIAM-4001, HIAM-4010, HIAM-4011, HIAM-4003, HIAM-4012, and HIAM-4013 along with simulated ones.

while DMA, DMF, and DEF were selected as solvents. The synthesis details are provided in the [Supporting Information](#).

Six different Zr-MOFs were obtained, in which HIAM-4001 and HIAM-4003 were previously synthesized. The BTTC linker led to two new types of Zr-MOFs. Truncated octahedron-shaped crystals of HIAM-4010 possess a (4,4,12)-c net, which is the same as we observed in HIAM-4008, while thinner and longer prismatic crystals of HIAM-4011 have a (4,8)-c **csq** net, which is the same as that of HIAM-4009. Similarly, for the linker NTTC, two new Zr-MOF structures were realized. Truncated octahedral crystals of HIAM-4012 and long prismatic crystals of HIAM-4013 possess the same topologies as HIAM-4008 and HIAM-4009 (Figure 4b). The phase purities from HIAM-4010 to HIAM-4013 were confirmed by the well agreed experimental PXRD patterns and the simulated ones generated from single crystal diffraction data of HIAM-4008 and HIAM-4009 (Figure 4c). The same reaction conditions as listed in Table S1 were used here, indicating that the proposed mechanism is generalized for similar tetratopic carboxylate linkers to realize customized synthesis. More importantly, all three luminescent MOFs (LMOFs) made of the same linker exhibit very similar solid-state emission behavior, while the observed emission shifts

were induced by the different packing of organic linkers in different nets (Figure S15). The similar effect on the PLQYs as we discussed from HIAM-4007 to HIAM-4009 was recorded for this series of LMOFs. For example, the highest PLQY is recorded for HIAM-4003 of 17.6%, and the lowest PLQY is observed for HIAM-4012 of 8.8% with the highest linker density under 365 nm excitation. These results further indicated that acid- and solvent-assisted topology evolution could be used for customized synthesis of MOFs with the best performance.

Table S4 lists topologies of various tetratopic carboxylate-based Zr-MOFs obtained under different reaction conditions. For each linker, one or two topologies among scu, csq, sqc, and scp are found. It should be noted that most of the MOFs adopt the same topologies as the HIAM-400X reported in the present work when the same solvent and acid were used, confirming that the proposed solvent- and acid-assisted topology evolution can be generalized. Note that introducing steric hindrance into the linker backbone or using linkers possessing a very different molecular structure from the one we used in the present study will also influence linker conformation and lead to different topology of the resulting MOFs under similar synthesis conditions.

CONCLUSIONS

In conclusion, a systematic investigation has been conducted to evaluate topology evolution in Zr-MOFs directed by synthetic conditions. Combination of three solvents and six acids yielded three different topologies of Zr-MOFs using only the same Zr₆ SBU and tetratopic carboxylate linker. The different structures show significant influence on the PLQY of resultant MOFs. Further experiments revealed that the basicity of solvents and the acidity of acids affected the structure of MOFs directly by modulating the protonation process of the organic linker and competition between the acid and linkers for coordination sites of the Zr₆ clusters. Rational selection of the acid and solvent is a key factor in directing MOF structures. This principle applies well to other tetratopic carboxylate linkers and represents a general approach for solvent- and acid-assisted topological evolution in Zr-MOFs. The current study may be helpful in establishing guidelines for the customized synthesis of MOFs for target-specific applications and enhanced performances.

ASSOCIATED CONTENT

Supporting Information

The Supporting Information is available free of charge at <https://pubs.acs.org/doi/10.1021/acs.inorgchem.2c00660>.

Material synthesis, characterizations, single crystal data, and other additional information (PDF)

Accession Codes

CCDC 2129023–2129024 contain the supplementary crystallographic data for this paper. These data can be obtained free of charge via www.ccdc.cam.ac.uk/data_request/cif, or by emailing data_request@ccdc.cam.ac.uk, or by contacting The Cambridge Crystallographic Data Centre, 12 Union Road, Cambridge CB2 1EZ, UK; fax: +44 1223 336033.

AUTHOR INFORMATION

Corresponding Authors

Xiao-Yuan Liu – Hoffmann Institute of Advanced Materials, Shenzhen Polytechnic, Shenzhen 518055, P.R. China;

orcid.org/0000-0003-2400-8085;

Email: liuxiaoyuan1989@szpt.edu.cn

Jing Li – Department of Chemistry and Chemical Biology, Rutgers University, Piscataway, New Jersey 08854, United States; Hoffmann Institute of Advanced Materials, Shenzhen Polytechnic, Shenzhen 518055, P.R. China; orcid.org/0000-0001-7792-4322; Email: jingli@rutgers.edu

Authors

Hai-Lun Xia – Hoffmann Institute of Advanced Materials, Shenzhen Polytechnic, Shenzhen 518055, P.R. China

Kang Zhou – Hoffmann Institute of Advanced Materials, Shenzhen Polytechnic, Shenzhen 518055, P.R. China

Liang Yu – Hoffmann Institute of Advanced Materials, Shenzhen Polytechnic, Shenzhen 518055, P.R. China

Hao Wang – Hoffmann Institute of Advanced Materials, Shenzhen Polytechnic, Shenzhen 518055, P.R. China;

orcid.org/0000-0001-7732-778X

Davide M. Proserpio – Dipartimento di Chimica, Università degli Studi di Milano, Milano 20133, Italy; orcid.org/0000-0001-6597-9406

Complete contact information is available at:

<https://pubs.acs.org/10.1021/acs.inorgchem.2c00660>

Notes

The authors declare no competing financial interest.

ACKNOWLEDGMENTS

H.-L. Xia gratefully acknowledges the funding support from Shenzhen Polytechnic (6021330018K). X.-Y. Liu acknowledges the financial support from start-up funding for Shenzhen High-Caliber Personnel of Shenzhen Polytechnic (6022310053K), the Shenzhen Science and Technology Program (RCBS20200714114941230), and the Guangdong Basic and Applied Basic Research Foundation (2020A1515110420).

REFERENCES

- (1) Furukawa, H.; Cordova, K. E.; O’Keeffe, M.; Yaghi, O. M. The chemistry and applications of metal-organic frameworks. *Science* **2013**, *341*, 1230444.
- (2) Feng, L.; Pang, J.; She, P.; Li, J. L.; Qin, J. S.; Du, D. Y.; Zhou, H. C. Metal-Organic Frameworks Based on Group 3 and 4 Metals. *Adv. Mater.* **2020**, *32*, 2004414.
- (3) Qian, Q.; Asinger, P. A.; Lee, M. J.; Han, G.; Mizrahi Rodriguez, K.; Lin, S.; Benedetti, F. M.; Wu, A. X.; Chi, W. S.; Smith, Z. P. MOF-Based Membranes for Gas Separations. *Chem. Rev.* **2020**, *120*, 8161–8266.
- (4) Adil, K.; Belmabkhout, Y.; Pillai, R. S.; Cadiau, A.; Bhatt, P. M.; Assen, A. H.; Maurin, G.; Eddaoudi, M. Gas/vapour separation using ultra-microporous metal-organic frameworks: insights into the structure/separation relationship. *Chem. Soc. Rev.* **2017**, *46*, 3402–3430.
- (5) Cui, Y.; Yue, Y.; Qian, G.; Chen, B. Luminescent Functional Metal-Organic Frameworks. *Chem. Rev.* **2012**, *112*, 1126–1162.
- (6) Lustig, W. P.; Mukherjee, S.; Rudd, N. D.; Desai, A. V.; Li, J.; Ghosh, S. K. Metal-organic frameworks: functional luminescent and photonic materials for sensing applications. *Chem. Soc. Rev.* **2017**, *46*, 3242–3285.
- (7) Chughtai, A. H.; Ahmad, N.; Younus, H. A.; Laypkov, A.; Verpoort, F. Metal-organic frameworks: versatile heterogeneous catalysts for efficient catalytic organic transformations. *Chem. Soc. Rev.* **2015**, *44*, 6804–6849.
- (8) Bavykina, A.; Kolobov, N.; Khan, I. S.; Bau, J. A.; Ramirez, A.; Gascon, J. Metal-Organic Frameworks in Heterogeneous Catalysis:

Recent Progress, New Trends, and Future Perspectives. *Chem. Rev.* **2020**, *120*, 8468–8535.

(9) Daglar, H.; Keskin, S. Recent advances, opportunities, and challenges in high-throughput computational screening of MOFs for gas separations. *Coord. Chem. Rev.* **2020**, *422*, 213470.

(10) Liang, B.; Li, B.; Li, Z.; Chen, B. Progress in Multifunctional Metal-Organic Frameworks/Polymer Hybrid Membranes. *Chem.—Eur. J.* **2021**, *27*, 12940–12952.

(11) Bosch, M.; Yuan, S.; Rutledge, W.; Zhou, H.-C. Stepwise Synthesis of Metal-Organic Frameworks. *Acc. Chem. Res.* **2017**, *50*, 857–865.

(12) Banerjee, R.; Phan, A.; Wang, B.; Knobler, C.; Furukawa, H.; O’Keeffe, M.; Yaghi, O. M. High-Throughput Synthesis of Zeolitic Imidazolate Frameworks and Application to CO₂ Capture. *Science* **2008**, *319*, 939–943.

(13) Deng, H.; Doonan, C. J.; Furukawa, H.; Ferreira, R. B.; Towne, J.; Knobler, C. B.; Wang, B.; Yaghi, O. M. Multiple Functional Groups of Varying Ratios in Metal-Organic Frameworks. *Science* **2010**, *327*, 846–850.

(14) Deng, H.; Grunder, S.; Cordova, K. E.; Valente, C.; Furukawa, H.; Hmadeh, M.; Gándara, F.; Whalley, A. C.; Liu, Z.; Asahina, S.; Kazumori, H.; O’Keeffe, M.; Terasaki, O.; Stoddart, J. F.; Yaghi, O. M. Large-pore apertures in a series of metal-organic frameworks. *Science* **2012**, *336*, 1018–1023.

(15) Lu, W.; Wei, Z.; Gu, Z.-Y.; Liu, T.-F.; Park, J.; Park, J.; Tian, J.; Zhang, M.; Zhang, Q.; Gentle III, T.; Bosch, M.; Zhou, H.-C. Tuning the structure and function of metal-organic frameworks via linker design. *Chem. Soc. Rev.* **2014**, *43*, 5561–5593.

(16) Ali Akbar Razavi, S.; Morsali, A. Linker functionalized metal-organic frameworks. *Coord. Chem. Rev.* **2019**, *399*, 213023.

(17) Cavka, J. H.; Jakobsen, S.; Olsbye, U.; Guillou, N.; Lamberti, C.; Bordiga, S.; Lillerud, K. P. A New Zirconium Inorganic Building Brick Forming Metal Organic Frameworks with Exceptional Stability. *J. Am. Chem. Soc.* **2008**, *130*, 13850–13851.

(18) Wu, S.; Ren, D.; Zhou, K.; Xia, H.-L.; Liu, X.-Y.; Wang, X.; Li, J. Linker Engineering toward Full-Color Emission of UiO-68 Type Metal-Organic Frameworks. *J. Am. Chem. Soc.* **2021**, *143*, 10547–10552.

(19) Mandal, S.; Natarajan, S.; Mani, P.; Pankajakshan, A. Post-Synthetic Modification of Metal-Organic Frameworks Toward Applications. *Adv. Funct. Mater.* **2021**, *31*, 2006291.

(20) Yuan, S.; Lu, W.; Chen, Y.-P.; Zhang, Q.; Liu, T.-F.; Feng, D.; Wang, X.; Qin, J.; Zhou, H.-C. Sequential Linker Installation: Precise Placement of Functional Groups in Multivariate Metal-Organic Frameworks. *J. Am. Chem. Soc.* **2015**, *137*, 3177–3180.

(21) Pang, J.; Di, Z.; Qin, J.-S.; Yuan, S.; Lollar, C. T.; Li, J.; Zhang, P.; Wu, M.; Yuan, D.; Hong, M.; Zhou, H.-C. Precisely Embedding Active Sites into a Mesoporous Zr-Framework through Linker Installation for High-Efficiency Photocatalysis. *J. Am. Chem. Soc.* **2020**, *142*, 15020–15026.

(22) Ren, D.; Xia, H. L.; Zhou, K.; Wu, S.; Liu, X. Y.; Wang, X.; Li, J. Tuning and Directing Energy Transfer in the Whole Visible Spectrum through Linker Installation in Metal-Organic Frameworks. *Angew. Chem., Int. Ed.* **2021**, *60*, 25048–25054.

(23) Dolgoplova, E. A.; Ejegbavwo, O. A.; Martin, C. R.; Smith, M. D.; Setyawan, W.; Karakalos, S. G.; Henager, C. H.; zur Loye, H.-C.; Shustova, N. B. Multifaceted Modularity: A Key for Stepwise Building of Hierarchical Complexity in Actinide Metal-Organic Frameworks. *J. Am. Chem. Soc.* **2017**, *139*, 16852–16861.

(24) Han, G.; Wu, S.; Zhou, K.; Xia, H.-L.; Liu, X.-Y.; Li, J. Full-Color Emission in Multicomponent Metal-Organic Frameworks via Linker Installation. *Inorg. Chem.* **2022**, *61*, 3363–3367.

(25) Eddaoudi, M.; Moler, D. B.; Li, H.; Chen, B.; Reineke, T. M.; O’Keeffe, M.; Yaghi, O. M. Modular Chemistry: Secondary Building Units as a Basis for the Design of Highly Porous and Robust Metal-Organic Carboxylate Frameworks. *Acc. Chem. Res.* **2001**, *34*, 319–330.

(26) Alexandrov, E. V.; Blatov, V. A.; Kochetkov, A. V.; Proserpio, D. M. Underlying nets in three-periodic coordination polymers: topology, taxonomy and prediction from a computer-aided analysis of

the Cambridge Structural Database. *CrystEngComm* **2011**, *13*, 3947–3958.

(27) Blatov, V. A.; Shevchenko, A. P.; Proserpio, D. M. Applied Topological Analysis of Crystal Structures with the Program Package ToposPro. *Cryst. Growth Des.* **2014**, *14*, 3576–3586.

(28) Li, H.; Eddaoudi, M.; O’Keeffe, M.; Yaghi, O. M. Design and synthesis of an exceptionally stable and highly porous metal-organic framework. *Nature* **1999**, *402*, 276–279.

(29) Eddaoudi, M.; Kim, J.; Rosi, N.; Vodak, D.; Wachter, J.; O’Keeffe, M.; Yaghi, O. M. Systematic Design of Pore Size and Functionality in Isorecticular MOFs and Their Application in Methane Storage. *Science* **2002**, *295*, 469–472.

(30) Loiseau, T.; Serre, C.; Huguenard, C.; Fink, G.; Taulelle, F.; Henry, M.; Bataille, T.; Férey, G. A rationale for the large breathing of the porous aluminum terephthalate (MIL-53) upon hydration. *Chem.—Eur. J.* **2004**, *10*, 1373–1382.

(31) Férey, G.; Mellot-Draznieks, C.; Serre, C.; Millange, F.; Dutour, J.; Surblé, S.; Margiolaki, I. A Chromium Terephthalate-Based Solid with Unusually Large Pore Volumes and Surface Area. *Science* **2005**, *309*, 2040–2042.

(32) Dan-Hardi, M.; Serre, C.; Frot, T.; Rozes, L.; Maurin, G.; Sanchez, C.; Férey, G. A New Photoactive Crystalline Highly Porous Titanium(IV) Dicarboxylate. *J. Am. Chem. Soc.* **2009**, *131*, 10857–10859.

(33) Luebke, R.; Belmabkhout, Y.; Weseliński, E. J.; Cairns, A. J.; Alkordi, M.; Norton, G.; Wojtas, L.; Adil, K.; Eddaoudi, M. Versatile rare earth hexanuclear clusters for the design and synthesis of highly-connected ftw-MOFs. *Chem. Sci.* **2015**, *6*, 4095–4102.

(34) Alezi, D.; Belmabkhout, Y.; Suyetin, M.; Bhatt, P. M.; Weseliński, E. J.; Solovyeva, V.; Adil, K.; Spanopoulos, I.; Trikalitis, P. N.; Emwas, A.-H.; Eddaoudi, M. MOF Crystal Chemistry Paving the Way to Gas Storage Needs: Aluminum-Based soc-MOF for CH₄, O₂, and CO₂ Storage. *J. Am. Chem. Soc.* **2015**, *137*, 13308–13318.

(35) Ma, J.; Tran, L. D.; Matzger, A. J. Toward Topology Prediction in Zr-Based Microporous Coordination Polymers: The Role of Linker Geometry and Flexibility. *Cryst. Growth Des.* **2016**, *16*, 4148–4153.

(36) Schneemann, A.; Bon, V.; Schwedler, I.; Senkovska, I.; Kaskel, S.; Fischer, R. A. Flexible metal-organic frameworks. *Chem. Soc. Rev.* **2014**, *43*, 6062–6096.

(37) Chen, Y.; Zhang, X.; Mian, M. R.; Son, F. A.; Zhang, K.; Cao, R.; Chen, Z.; Lee, S.-J.; Idrees, K. B.; Goetjen, T. A.; Lyu, J.; Li, P.; Xia, Q.; Li, Z.; Hupp, J. T.; Islamoglu, T.; Napolitano, A.; Peterson, G. W.; Farha, O. K. Structural Diversity of Zirconium Metal-Organic Frameworks and Effect on Adsorption of Toxic Chemicals. *J. Am. Chem. Soc.* **2020**, *142*, 21428–21438.

(38) Chen, Z.; Hanna, S. L.; Redfern, L. R.; Alezi, D.; Islamoglu, T.; Farha, O. K. Reticular chemistry in the rational synthesis of functional zirconium cluster-based MOFs. *Coord. Chem. Rev.* **2019**, *386*, 32–49.

(39) Wang, B.; Lv, X.-L.; Feng, D.; Xie, L.-H.; Zhang, J.; Li, M.; Xie, Y.; Li, J.-R.; Zhou, H.-C. Highly Stable Zr(IV)-Based Metal-Organic Frameworks for the Detection and Removal of Antibiotics and Organic Explosives in Water. *J. Am. Chem. Soc.* **2016**, *138*, 6204–6216.

(40) Pang, J.; Yuan, S.; Qin, J.; Liu, C.; Lollar, C.; Wu, M.; Yuan, D.; Zhou, H.-C.; Hong, M. Control the Structure of Zr-Tetracarboxylate Frameworks through Steric Tuning. *J. Am. Chem. Soc.* **2017**, *139*, 16939–16945.

(41) Wang, B.; Yang, Q.; Guo, C.; Sun, Y.; Xie, L.-H.; Li, J.-R. Stable Zr(IV)-Based Metal-Organic Frameworks with Predesigned Functionalized Ligands for Highly Selective Detection of Fe(III) Ions in Water. *ACS Appl. Mater. Interfaces* **2017**, *9*, 10286–10295.

(42) Carter, J. H.; Han, X.; Moreau, F. Y.; da Silva, I.; Nevin, A.; Godfrey, H. G. W.; Tang, C. C.; Yang, S.; Schröder, M. Exceptional Adsorption and Binding of Sulfur Dioxide in a Robust Zirconium-Based Metal-Organic Framework. *J. Am. Chem. Soc.* **2018**, *140*, 15564–15567.

(43) Wang, H.; Dong, X.; Colombo, V.; Wang, Q.; Liu, Y.; Liu, W.; Wang, X. L.; Huang, X. Y.; Proserpio, D. M.; Sironi, A.; Han, Y.; Li, J. Tailor-Made Microporous Metal-Organic Frameworks for the Full

Separation of Propane from Propylene Through Selective Size Exclusion. *Adv. Mater.* **2018**, *30*, 1805088.

(44) Schaate, A.; Roy, P.; Godt, A.; Lippke, J.; Waltz, F.; Wiebcke, M.; Behrens, P. Modulated Synthesis of Zr-Based Metal-Organic Frameworks: From Nano to Single Crystals. *Chem.—Eur. J.* **2011**, *17*, 6643–6651.

(45) Wißmann, G.; Schaate, A.; Lilienthal, S.; Bremer, I.; Schneider, A. M.; Behrens, P. Modulated synthesis of Zr-fumarate MOF. *Microporous Mesoporous Mater.* **2012**, *152*, 64–70.

(46) Wasson, M. C.; Lyu, J.; Islamoglu, T.; Farha, O. K. Linker Competition within a Metal-Organic Framework for Topological Insights. *Inorg. Chem.* **2019**, *58*, 1513–1517.

(47) Hu, Z.; Wang, Y.; Zhao, D. The chemistry and applications of hafnium and cerium(IV) metal-organic frameworks. *Chem. Soc. Rev.* **2021**, *50*, 4629–4683.

(48) Chun, A. Y.; Yunxiao, L.; Ashok, S.; Seol, E.; Park, S. Elucidation of toxicity of organic acids inhibiting growth of *Escherichia coli* W. *Biotechnol. Bioprocess Eng.* **2014**, *19*, 858–865.

(49) Pytela, O.; Prusek, O. Chemometric Analysis of Substituent Effects. XII. Application of Relationship Between 2- and 4-Substitution of Benzene Ring to Study ortho Effect in Selected Compounds with Different Reaction Centres. *Collect. Czech. Chem. Commun.* **1999**, *64*, 1617–1628.

(50) Adelman, R. L. Studies on the Base Strengths of N,N-Disubstituted Amides. *J. Org. Chem.* **1964**, *29*, 1837–1844.